ACS OMEGA

http://pubs.acs.org/journal/acsodf

Article

# Cortisol Detection in Undiluted Human Serum Using a Sensitive Electrochemical Structure-Switching Aptamer over an Antifouling Nanocomposite Layer

Naveen K. Singh, Saeromi Chung, Michael Sveiven, and Drew A. Hall*

Cite This: *ACS Omega* 2021, 6, 27888−27897

Read Online

ACCESS | Metrics & More | Article Recommendations | Supporting Information

**ABSTRACT:** There is a strong and growing need to monitor stress biomarkers *in vivo* for real-time emotional and wellness assessment. Toward this, we report a reagent-free electrochemical aptasensor with a nanocomposite antifouling layer for sensitive and continuous detection of cortisol in human serum. A thiolated, methylene blue (MB)-tagged conformation-switching aptamer was immobilized over a gold nanowire (AuNW) nanocomposite to capture cortisol and generate a signal proportional to the cortisol concentration. The signal is recorded through differential pulse voltammetry (DPV) and chronoamperometry. The aptasensor exhibited a sensitive response with 0.51 and 0.68 nM detection limits in spiked buffer and undiluted serum samples, respectively. Interference from other structurally similar analogs, namely, epinephrine and cholic acid, was negligible (<10%). The developed nanocomposite-based aptasensor showed excellent stability in undiluted human serum, outperforming several other nanocomposite materials even after prolonged exposure. This work lays the foundation for new biosensor formats such as implantable and wearable sensors.

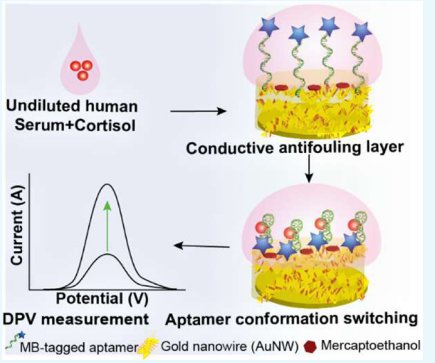


## INTRODUCTION

Stress affects the physical and mental health of everyone. It is recognized as a major risk factor and a silent contributor to various health-related disorders.[1] The American Institute of Stress reported that 120 000 deaths per year are directly caused by stress and that stress leads to an annual economic burden of more than $200 billion.[2] The number of stress-related health disorders has increased significantly over the last decade[3] and will likely see a significant spike due to the added pressures of COVID-19. Stress comes in many forms, from long-term, chronic stress caused by workload or health issues to short-term, extreme situations such as the flight or fight reaction caused by life-threatening situations.[4] An individual's physical and emotional makeup can escalate or de-escalate the effects of stress.[5] Continuous or routine monitoring of stress levels is a vital yet neglected aspect of our health, especially for high-stress professions (*e.g.*, military, law enforcement, and emergency personal), athletes, and people with pre-existing medical conditions.

The human body responds to stress by modulating the release of hormones that alter the biochemistry of the whole body.[6] Thus, hormones provide a view into the nervous system and serve as powerful biomarkers, specifically serotonin, epinephrine, norepinephrine, and cortisol.[1] Among these, cortisol is a very attractive biomarker as it is present in high concentrations in various bodily fluids (blood, urine, saliva, and interstitial fluid), and its concentration directly fluctuates with the individual's stress level.[7] Cortisol is a glucocorticoid hormone secreted by the adrenal gland. It follows the circadian rhythm (also known as the natural sleep−wake cycle) and works in cohort with other hormones in the neuroendocrine system. Besides stress, increased cortisol levels are linked to other disorders such as inflammation, irritable bowel syndrome, chronic fatigue syndrome, and post-traumatic stress disorder.[8,9] Moreover, cortisol is highly active, has a low molecular weight (362 Da), is released directly in an unbound form, and has a rapid response time compared to other stress biomarkers. Cortisol is rapidly cleared from circulation, unlike larger stress biomarkers, which provides a more real-time assessment.[1,10] While cortisol is secreted directly into blood (100−600 nM), it is found in other biofluids as well, such as sweat (22−392 nM), urine (27−276 nM), and saliva (2.7−4.4 nM).[11−13]

Currently, cortisol is detected via a spectrophotometric (absorbance or fluorometric) assay,[14] high-performance liquid chromatography (HPLC),[15] liquid chromatography-mass spectroscopy (LC-MS),[16] enzyme-linked immunosorbent assay (ELISA), or surface plasmon resonance (SPR).[17,18] These techniques tend to be time-consuming, require skilled

**Received:** July 6, 2021
**Accepted:** September 16, 2021
**Published:** October 11, 2021

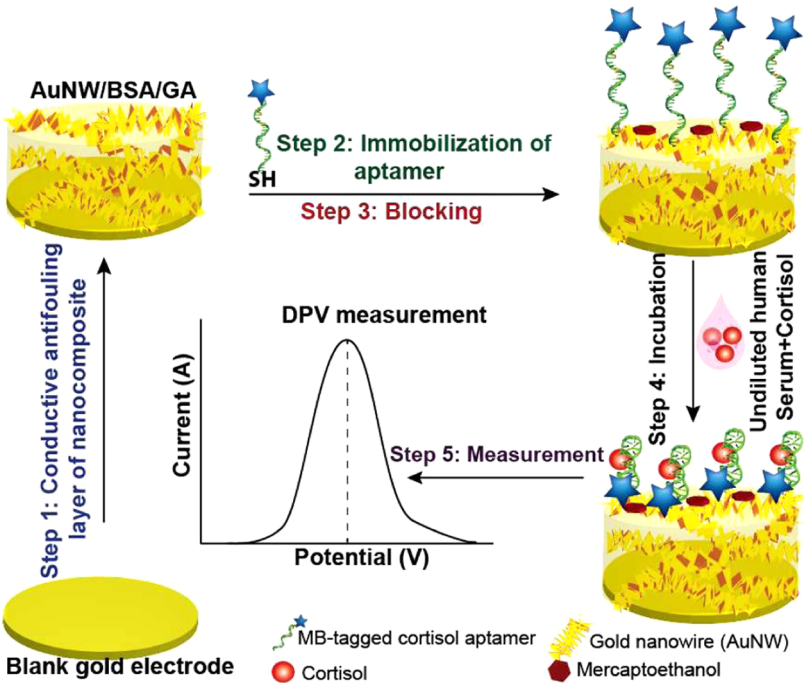


**Figure 1.** Overview of aptasensor fabrication and cortisol measurement. (Step 1) Synthesis of antifouling nanocomposite layer (BSA/AuNW/GA) on a gold electrode. (Step 2) Immobilization of MB-tagged, thiolated cortisol aptamer, followed by (Step 3) blocking with mercaptoethanol. (Step 4) Incubation with sample and (Step 5) DPV measurement.

personnel, and are instrument-dependent, leaving them laboratory-bound. Recently, electrochemical-based assays have gained popularity due to their low cost, high sensitivity, and high level of integration, especially in portable form factors.[19−24] While most electrochemical techniques use an assay similar to ELISAs, a new format using affinity reagents with conformation-changing properties is appealing since the electroactive reporter can be directly conjugated to the probe molecule, removing the need for a second recognition element.[25−27] Aptamers are single-stranded oligonucleotides developed through systemic evaluation of ligand by exponential enrichment process (SELEX) with a high affinity toward the target molecule.[28] They have advantages in terms of stability, cost, shelf-life, and ease of chemical modifications compared to traditional antibody-based systems.[29,30] Furthermore, aptamers can be engineered to have a conformation-switching property that allows them to modulate the label's position during a binding event when labeled with a redox-active molecule.[26,31,32] These properties make conformation-changing aptamers attractive for wash-free, reagent-less, continuous monitoring applications.

In the last decade, many aptamer-based electrochemical sensors have been reported with various surface chemistries.[33−35] However, successful commercialization for clinical diagnostic applications has been impeded by surface biofouling where when exposed to complex matrices such as saliva, serum, or blood,[35] nonspecific binding on the sensor surface affects the sensor performance. While well-established antifouling coating strategies such as poly(ethylene glycol) (PEG) or oligo ethylene glycol with BSA or peptides[34] prevent nonspecific adsorption, they also inhibit electron transfer and thus signaling for some sensors. The nanoengineered conductive antifouling layer is an alternative structure to prevent biofouling without hindering the electron transfer.[36] This allows one to make a reliable, continuous monitoring aptasensor, as demonstrated in this work.

This paper reports an electrochemical sensor based on a conformation-changing aptamer atop a conductive antifouling nanocomposite surface to detect cortisol in undiluted human serum, as shown in Figure 1. The conductive antifouling layer comprising gold nanowires (AuNWs) and bovine serum albumin (BSA) cross-linked with glutaraldehyde (GA) facilitates high-efficiency electron transfer while minimizing nonspecific binding. The aptasensor performance is demonstrated with spiking studies, temporal kinetic response, and sensor stability in serum. We demonstrate, for the first time, an integrated conductive antifouling layer with a conformation-switching aptamer for reagent-less detection of cortisol enabling rapid quantification. The aptasensor achieved comparable performance to the best-performing cortisol assay with the significant advantage of detection in undiluted serum without any sample pretreatment, potentially allowing it to be used for *in vivo* and wearable, continuous monitoring applications.

## MATERIALS AND METHODS

**Reagents and Instruments.** Methylene blue (MB)-tagged, thiolated, HPLC-grade purified aptamer was ordered from LGC, Biosearch Technologies. The sequence was 5′-SH $(CH_2)_6$-*T TTT* AGC AG C ACA GAG GTC AGA TGC AAA CCA CAC CTG AGT GGT TAG CGT ATG TCA TTT ACG GC *TTT T*-MB 3MB.[37] At both ends of the aptamer, tetrathymine (illustrated in italics) oligonucleotides were attached as a linker region to support the native conformation after immobilization on the gold surface. The selected aptamer has a binding affinity ($K_d$) of 6.9 ± 2.8 $\mu$M,[37] and its clinical significance has been validated by several research groups.[38−43] Another cortisol binding aptamer with a $K_d$ of 30 nM[44] was reported recently,[13] but its conformation-switching property


https://doi.org/10.1021/acsomega.1c03552
ACS Omega 2021, 6, 27888−27897

on target binding still needs to be investigated. The aptamer binding buffer and measurement buffer compositions are described in Supporting Information Table S1. Phosphate buffer saline (PBS), NaCl, $MgCl_2$, KCl, bovine serum albumin (BSA), 4500 × 30 $nm^2$ gold nanowire (AuNW) (#716944), a 15 nm diameter reactant-free gold nanoparticle (AuNP) suspended in PBS (#777099), 6-mercapto-1-hexanol (MCH; #451088), $\beta$-mercaptoethanol (#6250), sulfuric acid (#339741), and human serum from AB-positive males were purchased from Sigma-Aldrich. Gold nanospheres (AuNSs) (#790128-010) with a 250 nm diameter were obtained from Corpuscular, Inc. Alumina powder (50 nm core size) was procured from CH Instruments, Inc. All analytical-grade reagents such as cortisol, cholic acid, epinephrine, and glucose were obtained from Sigma-Aldrich. Glutaraldehyde (GA) was purchased from Spectrum Chemicals. Tris(2-carboxyethyl)-phosphine (TCEP; #77720) bond-breaker solution was ordered from Thermo Fisher Scientific.

Differential pulse voltammetry (DPV), chronoamperometry (CA), cyclic voltammetry (CV), and electrochemical impedance spectroscopy (EIS) measurements were performed using a benchtop potentiostat (CH Instruments, 750E). A three-electrode setup was used for all experiments with Au (BASI, #MF-2114), Ag/AgCl (BASi), and Pt wires (CH Instruments, #CHI115) as the working electrode (WE), reference electrode (RE), and counter electrode (CE), respectively.

**Electrode Cleaning.** Bare gold electrodes (3 mm diameter) were chemically cleaned in piranha solution (3:1 ratio of $H_2SO_4/H_2O_2$; safety note: piranha is a highly corrosive solution and requires extreme caution during handling) for 1 min followed by mechanical cleaning with a slurry of 50 nm alumina particles on a polishing pad (BASi) by rubbing in a figure-eight pattern for 5 min each, sequentially. Alumina particles adhered to the electrodes were removed by sonication in ethanol and ultrapure water (HPLC grade) for 5 min each, successively. Afterward, electrodes were electrochemically cleaned in 0.5 M $H_2SO_4$ by sweeping the potential between −0.5 and 1.4 V versus Ag/AgCl until a steady characteristic redox current peak was observed. The electrodes were then washed with ultrapure water and air-dried.

**Preparation of the Nanocomposite and Reduction of the Thiolated MB-Tagged Aptamer.** The antifouling layer on the electrode composed of a nanocomposite with conductive properties was prepared using a previously reported method[45] with minor modifications. Briefly, 5 mg of BSA was dissolved through gentle pipetting in 1 mL of AuNW in $H_2O$, followed by sonication for 5 min in a water bath. The resulting nanocomposite solution was stored at 4 °C for later use. The thiol-modified aptamer was received in an oxidized form and protected with a disulfide (S−S) bond. One hundred micromolar of TCEP solution was added to 10 $\mu$M of aptamer, suspended in binding buffer, and incubated for 1 h at room temperature to reduce the disulfide bond. The reduced aptamer was used for sensor fabrication without purification.

**Sensor Fabrication.** Clean gold electrodes were incubated in 79 $\mu$L of antifouling nanocomposite solution consisting of 69 $\mu$L of the nanocomposite with 10 $\mu$L of a 25% GA solution and left for 24 h in a humidity chamber. The surface-modified electrodes (Au/BSA/AuNW/GA or Au/NC) were washed with 1× PBS (pH 7.4) in a shaker for 30 min followed by a CV scan (−0.5 to 0.8 V at 0.1 V/s) in measurement buffer for surface activation and again washed with ultrapure water. Fifty microliters of a 2 $\mu$M reduced thiolated MB-tagged aptamer in binding buffer was incubated with the NC-layered electrode for 16 h in a humidity chamber. After immobilization, the unbound aptamer was washed with binding buffer. To further ensure proper coverage of the exposed electrode surface, the electrodes were treated with 1 mM of $\beta$-mercaptoethanol in binding buffer for 15 min. The aptasensor was again washed with ultrapure water and then air-dried.

**Atomic Force Microscopy (AFM).** Topological characterization of the sensor surface to determine morphology and roughness of the antifouling layer was performed by AFM in continuous tapping mode with a <7 nm radius curvature tip using a Veeco scanning probe microscope (Cypher, Asylum Research; DI-3100, Veeco). Data analysis was performed with WsxM v5.

**Electrochemical Characterization of Aptasensor.** A layer-by-layer assembly of the aptasensor was characterized by CV and EIS measurements. EIS spectra were recorded with a 5 mV ac amplitude from 1 Hz to 1 MHz. The resulting curves were fit with Z-view (Scribner Associates). Voltammograms were measured using CV from −0.5 to 0.8 V at a 0.1 V/s scan rate with a 1 mV sample interval. All electrochemical measurements were performed in 10 mM $[Fe(CN)_6]^{4-/3-}$ with 0.2 M KCl in PBS solution, pH 7.4.

**Calculation of the Electron Transfer Rate.** The MB-tagged aptamer has a variable distance from the electrode surface before and after binding with cortisol, which affects the electron transfer rate ($k_{ET}$) between the redox molecules and the surface. This rate was calculated using Laviron's method.[46,47] The difference ($\Delta E_p$) between the anodic ($E_{pa}$) and cathodic ($E_{pc}$) peak potentials at different logarithmic scan rates ($\nu$) was used to calculate $k_{ET}$ and the transfer coefficient ($\alpha$) using

$$\Delta E_p = E^0 + \left(\frac{RT}{\alpha nF}\right)\left[\ln\left(\frac{RT\ k_{ET}}{\alpha nF}\right) - \ln \nu\right] \quad (1)$$

where $E_0$ is the perceptible midpoint potential of the redox species, $n$ is the number of electrons transferred ($n$ = 2 for MB), $R$ is the gas constant, $T$ is the temperature, $F$ is Faraday's constant, and $\alpha$ is the transfer coefficient representing the measure of the symmetry of the activation barrier.

**Cortisol Assay.** Before the measurement, the aptasensor was equilibrated in the measurement buffer until a stable voltammogram signal was observed. It was then incubated for 30 min in 200 $\mu$L of binding buffer or serum spiked with varying cortisol concentrations. Experiments with human serum were performed without any processing or pretreatment. The sensor was gently washed with binding buffer, and DPV measurements were taken in the measurement buffer. DPV measurements were collected from −0.45 to 0.1 V in 5 mV steps with a 100 mV amplitude, a 50 ms pulse width, a 20 ms sample width, and a 500 ms pulse period. The specificity assays followed the same process but with competitive targets, namely, epinephrine, cholic acid, and other significant serum constituents such as glucose. Chronoamperometry experiments were carried out with continuous stirring at 200−300 rpm and a constant potential of 0.26 V versus Ag/AgCl by supplementing cortisol.

**Statistical Analysis.** All data shown are the mean values with 1 standard deviation as error bars. Data were obtained from three experiments performed with independent sensors fabricated and examined under similar conditions. Origin v9.0 was used for statistical analysis. The limit of detection (LOD)


https://doi.org/10.1021/acsomega.1c03552
ACS Omega 2021, 6, 27888−27897

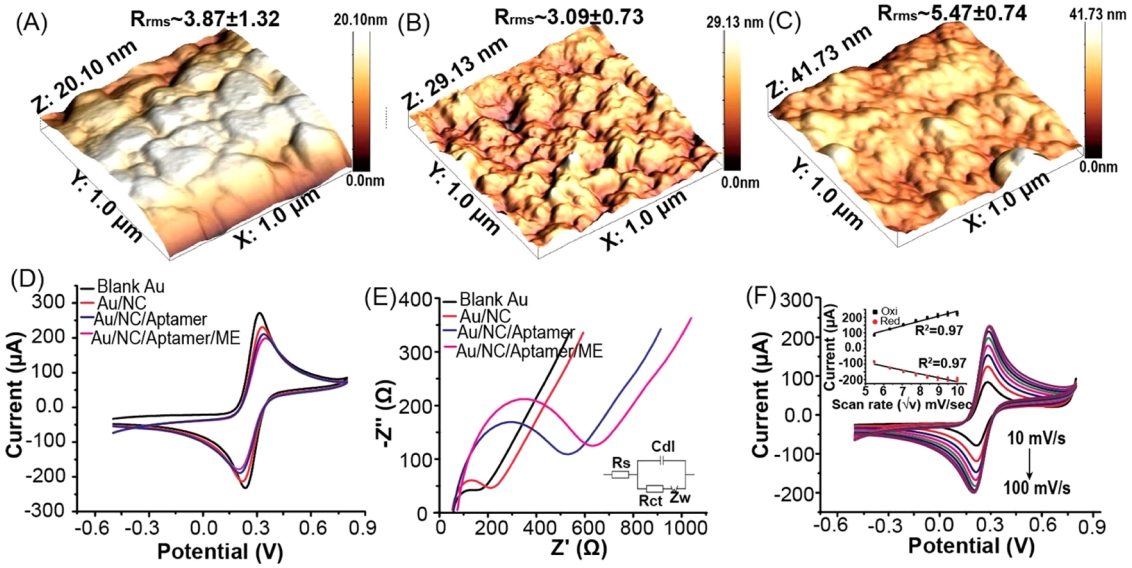


**Figure 2.** Sensor surface characterization. AFM images of the (A) bare gold electrode, (B) nanocomposite layer of BSA/AuNW/GA over the gold electrode, and (C) aptamer immobilization on the nanocomposite layer. Electrochemical characterization of the fabrication process using (D) CV and (E) EIS. (F) Measured voltammograms at different scan rates. The inset shows the extracted redox peak mean current versus the square root of the scan rate.

was calculated using the slope method, where LOD = 3 × standard deviation (SD) of the blank/slope.[48] The kinetic constants were extracted using Graphpad Prism (v9.1).

## RESULTS AND DISCUSSION

**Sensor Surface Characterization.** The aptasensor was fabricated by depositing a nanocomposite (NC) layer consisting of gold nanowires (AuNWs), proteins, and a cross-linker (glutaraldehyde) over a gold electrode. The aptamer was then covalently linked via the thiol groups on the aptamer and AuNW. The stepwise fabrication process was characterized by AFM. Figure 2A–C shows measured topographical and morphological features on the sensor surface for a bare electrode, an electrode coated with the nanocomposite material, and a fully functionalized sensor consisting of the nanocomposite, aptamer, and blocking layers. As expected, the surface roughness decreased after the nanocomposite layer and then increased after the aptamer and blocking layers. Cross-sectional images are shown in Supporting Information Figure S1 to provide further evidence of the proper layer-by-layer assembly. The AFM images demonstrate that the electrode is well constructed and homogeneous with no large aggregates or defects.

The sensor's electrochemical characteristics were then investigated by CV and EIS in a redox buffer containing 10 mM of ferri-/ferrocyanide, $[Fe(CN)_6]^{4-/3-}$. Figure 2D shows the gradual reduction of the redox peak due to the reduced electron transport after each layer's addition. The NC layer provides a 3D scaffold with excellent antifouling properties while not significantly hindering the electron transfer.[45] Compared to a BSA/AuNW passivation layer, the NC led to significantly less reduction in the oxidation/reduction peak currents (Supporting Information Figure S2A) and was thus selected for all subsequent sensors. Immobilizing the thiolated aptamer on the NC layer reduces the oxidation/reduction peak currents due to the charge repulsion from the aptamer's negative phosphate backbone and the partial surface passivation.[49] Finally, the surface was blocked with β-mercaptoethanol (2ME) to passivate the surface. A slight decrease in redox current was observed due to the blocking of pinhole islands over the sensor surface by 2ME, *i.e.* small, planar insulated molecules. These data indicate successful aptamer immobilization and blocking of the gold electrode surface.

EIS was used as a confirmatory technique to verify the functionalization. Nyquist plots fitted with a Randles–Ershler equivalent circuit model are shown in Figure 2E. The charge-transfer resistance ($R_{ct}$) increased from 120 ± 12 Ω for the blank gold electrode to 152 ± 25 Ω after immobilization of the NC layer. The subsequent aptamer immobilization and blocking further increased the impedance to 470 ± 39 and 687 ± 32 Ω, respectively. The stepwise reduction in the oxidation/reduction peak current and increase in $R_{ct}$ indicate successful fabrication of the aptasensor.

The electron transport rate from the redox molecules through the sensor surface was assessed by measuring voltammograms at different scan rates, ranging from 10 to 100 mV/s (Figures 2F and S2B). The oxidation and reduction currents increased linearly with the square root of the scan rate. The presence of an electroactive species, Γ, at the electrode surface was calculated with Faraday's law, $Q = nFA\Gamma$, where $F$ is Faraday's constant (96 485 C/mol), $A$ is the electrode area (0.07 $cm^2$), $n$ is the number of electrons, and $Q$ is calculated by integrating the anodic peak at 30 mV/s (similar oxidation and reduction peaks). Γ was found to be $1.33 \times 10^{-8}$ and $9.9 \times 10^{-9}$ mol·$cm^2$ for the blank and aptamer-modified electrodes, respectively. A slight reduction in the redox species' surface concentration was observed for the aptamer NC-modified electrode, indicating a diffusion-limited process instigated by electrostatic repulsion from the aptamer's phosphate backbone.

**Optimization of the Aptamer Density and Incubation Time.** The aptamer density on the sensor surface plays a critical role in determining the overall sensor performance. Loosely packed aptamers significantly reduce the signal, especially in redox-labeled conformation-switching aptamers.[50] In contrast, densely packed aptamers can cause steric


https://doi.org/10.1021/acsomega.1c03552
ACS Omega 2021, 6, 27888–27897

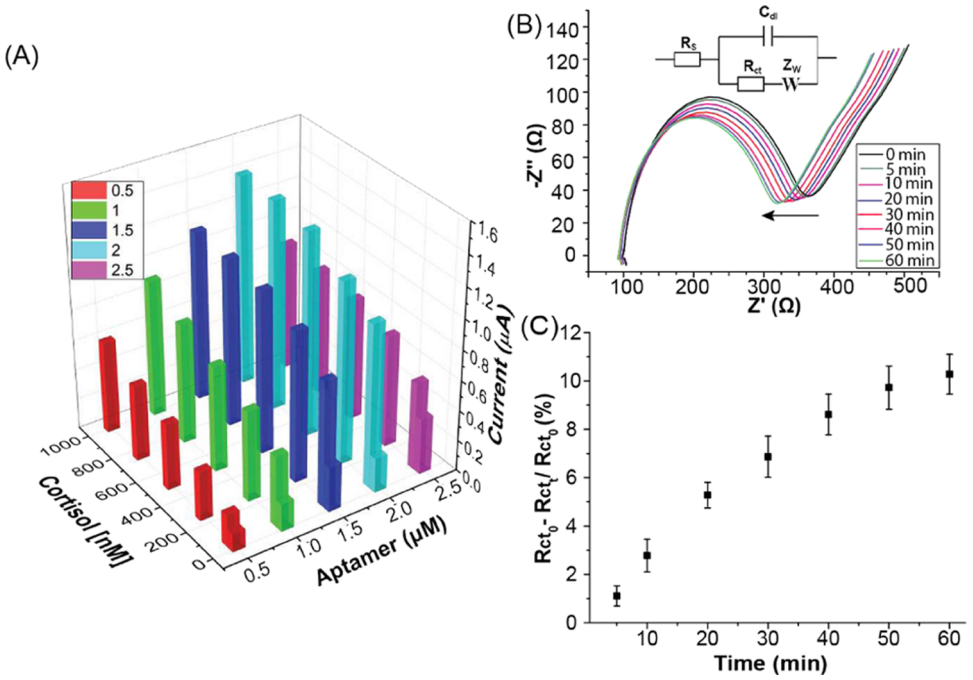


**Figure 3.** Optimization of the aptamer density and incubation time. (A) Signal recorded by DPV with cortisol (1 $\mu$M) spiked in binding buffer at various aptamer concentrations (0.5, 1.0, 1.5, 2, 2.5 $\mu$M). (B) Binding time optimization study through EIS using Nyquist plots, fitted with the Randles equivalent circuit, where $R_s$ is the solution resistance, $Z_w$ is the Warburg diffusion impedance, and $C_{dl}$ is the double-layer capacitance. (C) Change in $R_{ct}$ versus the binding time.

hindrance and not provide enough space to allow the aptamer to adopt a suitable 3D conformation resulting in reduced binding efficiency.[51] The surface coverage was studied through a matrix of experiments to maximize the electrochemical response. The best response was obtained with 2 $\mu$M of aptamer across the entire range of cortisol concentrations (Figure 3A). Higher concentrations resulted in a lower signal, as expected from the previous discussion. EIS was used to optimize the incubation time with 1 $\mu$M of the cognate protein. The data in Figure 3B show $R_{ct}$ decreasing over time as the binding to cortisol brings the redox reporter close to the surface, reducing the charge-transfer resistance. $R_{ct}$ increased linearly for the first 30 min (point of inversion) and then started to plateau (Figure 3C). These conditions were used for all subsequent assays.

**Cortisol Detection.** The proposed aptasensor strategy for enhanced antifouling properties and reagent-less sensitive cortisol detection through a conformation-switching aptamer is illustrated in Figure 1. The enhanced sensitivity and antifouling property are reinforced by the immobilization of the aptamer on an NC matrix. BSA (pI ~4.7) in the NC prevents the sensor surface from biofouling via charge repulsion, whereas the AuNW functions as a nanowire to sustain electron transfer from the MB-tagged aptamer. Aptamer conformation switching occurs when binding with cortisol, and the ostensible distance between distal-appended MB and electrode surface decreases. Such conformational changes instigate a fast interfacial rate of electron transfer ($k_{ET}$) from 13.6 to 40.7 $s^{-1}$ between the redox molecule and the electrode surface, as calculated from the Laviron equation before and after interaction with cortisol (Supporting Information Figure S5A). Based on this principle, we measured contrived samples by spiking cortisol into a buffer or undiluted human serum and incubating the sample on the aptasensor for 30 min. The sensor response was observed using DPV with the typical MB oxidation peak (−260 mV), as shown in Figure 4. The aptasensor response exhibited a monotonic increase in peak current with increasing cortisol concentration between 1 and 1000 nM in buffer (Figure 4A) and undiluted human serum (Figure 4C). The gradual current increase results from the accumulation of MB near the sensor surface due to cortisol binding with the structure-switching aptamer. Compared to larger targets (*e.g.*, proteins), small molecules like cortisol have better accessibility to the aptamer and greatly benefit from the confirmation-switching property.[52] The background signal in the control trace (buffer) is likely due to the MB-tagged aptamer's misorientation on the electrode surface. This background signal is further increased in serum due to the basal cortisol level in the pooled serum as no attempt was made to deplete it. As depicted in Figure 4A,C, a slight peak shift was observed and attributed to the binding of partially charged cortisol[44,53] with the MB-tagged aptamer. The modified Nernst equation,[54] $E^{0\prime} = E^0 + \phi_{pet} - \phi_s$, explains this, where $E^{0\prime}$ is the formal potential, $E^0$ is the standard electrode potential, $\phi_s$ is the solution potential, and $\phi_{pet}$ is the potential of the electron transfer plane, *i.e.* the plane where the electroactive molecule lies. It is clear from this equation that the solution potential remains constant in a fixed ionic strength solution; however, a change in $\phi_{pet}$ takes place upon binding of a charged molecule and leads to a peak shift.

Calibration curves were generated by compiling the aptasensor responses from varying cortisol concentrations, as shown in Figure 4B,D. A linear detection range from 1 to 1000 nM for contrived samples in both buffer and serum was observed, covering the physiological cortisol range of 100−600 nM in humans.[7] Further extending the concentrations beyond this range to get saturation is not significant as per clinical requirements. A linear response calibration model is preferred


https://doi.org/10.1021/acsomega.1c03552
ACS Omega 2021, 6, 27888−27897

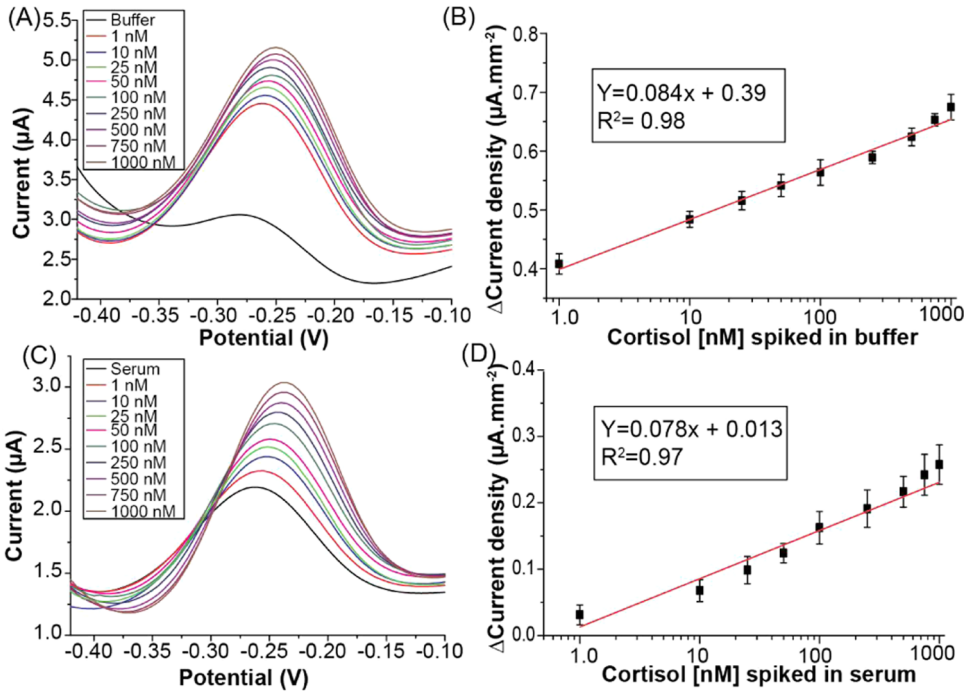


**Figure 4.** Spiked cortisol detection in buffer and undiluted human serum. Measured voltammograms using DPV with aptasensor at different concentrations of cortisol spiked in (A) buffer and (C) undiluted human serum with the corresponding calibration curves (B) and (D), respectively.

for biosensing over other models (curvilinear or nonlinear) due to its implementation simplicity.[55] A slightly lower sensitivity was seen in serum, likely due to the presence of off-target proteins, different ionic strength, and different conductivity compared to that of buffer.[56] More importantly, repeated measurements were highly reproducible and consistent. We measured a high signal-to-noise ratio compared to the background, which varies from 22 to 74 times in buffer and 6 to 48 times in serum from the lowest (1 nM) to the highest (1000 nM) cortisol concentration (Supporting Information Figure S3A). The limit of detection (LOD) was calculated to be 0.51 and 0.68 nM in buffer and undiluted human serum, respectively, whereas the sensitivity was 84.0 and 78.0 nA/mm$^2$/[cortisol/nM] in buffer and serum, respectively. Both calibration curves had very linear fits ($R^2$ > 0.97). These data demonstrate the ability to detect cortisol in both buffer and undiluted human serum with high sensitivity across the physiological range.

Analytical performance validation was performed using the recovery ratio method[57] and compared with standard systems such as absorbance and fluorescence spectroscopy (Supporting Information Figure S3B). The recovery of cortisol from a spiked sample with the aptasensor was 98.7%, compared to 98.1 and 102% in absorbance and fluorescence spectroscopies, respectively (Supporting Information Table S2). This established the sensing accuracy relative to standard spectroscopy methods. The intra- and interbatch relative standard deviations (RSDs) were 3.45 and 5.68%, respectively (Supporting Information Figure S4A). The low RSD values (<10%) demonstrate the aptasensor's precision. Reusability was studied using 1× PBS with 1 M NaCl at pH 4.5 for 15 min. The aptasensor was successfully regenerated 3× without significant loss in binding efficiency (Supporting Information Figure S4B). The slight reduction (∼8%) in aptamer regeneration efficiency compared to preliminary binding may be due to repetitive exposure to low pH solution of highly concentrated salt.

**Specificity and Stability in Human Serum.** Interference due to off-target proteins and/or small molecules in serum is a significant problem for many biosensors. Having already demonstrated cortisol detection in undiluted human serum, we screened for interference using structural analogs of cortisol such as epinephrine and cholic acid, as well as glucose since its level is regulated by cortisol. Each of these potential interferents was spiked in buffer at a concentration of 1000 nM and measured using the same optimized parameters previously described (Figure 5A). The signal was much lower (<10%) than the target molecule spiked in at the same concentration in each case. These data demonstrate the aptamer's selectivity to correctly bind the cognate molecule, even in the presence of closely related analogs.

Sensor stability is a prerequisite for clinical diagnostic applications. We performed measurements where the sensor was exposed to serum for an extended duration to demonstrate the sensor's stability and antifouling properties. For comparison, we constructed aptasensors with gold nanospheres (AuNSs), gold nanowires (AuNWs), and gold nanoparticles (AuNPs) in equal densities by drop-casting on a clean gold electrode. The electrodes were then functionalized using the previously described protocol. The layer-by-layer assembly was characterized by CV (Supporting Information Figure S5B−D) and DPV (Supporting Information Figure S6). The results confirmed the successful fabrication of nanomaterial-based aptamer sensors. The signal due to cortisol was investigated before and after a 3 h incubation in serum, as shown in Figure 5B. The responses were normalized to the initial signal to remove the conductivity differences. After 3 h, reduced sensor performance was observed for all other nanomaterials except the Au/NC/Au layer, demonstrating superior stability and antifouling properties.



https://doi.org/10.1021/acsomega.1c03552
ACS Omega 2021, 6, 27888−27897

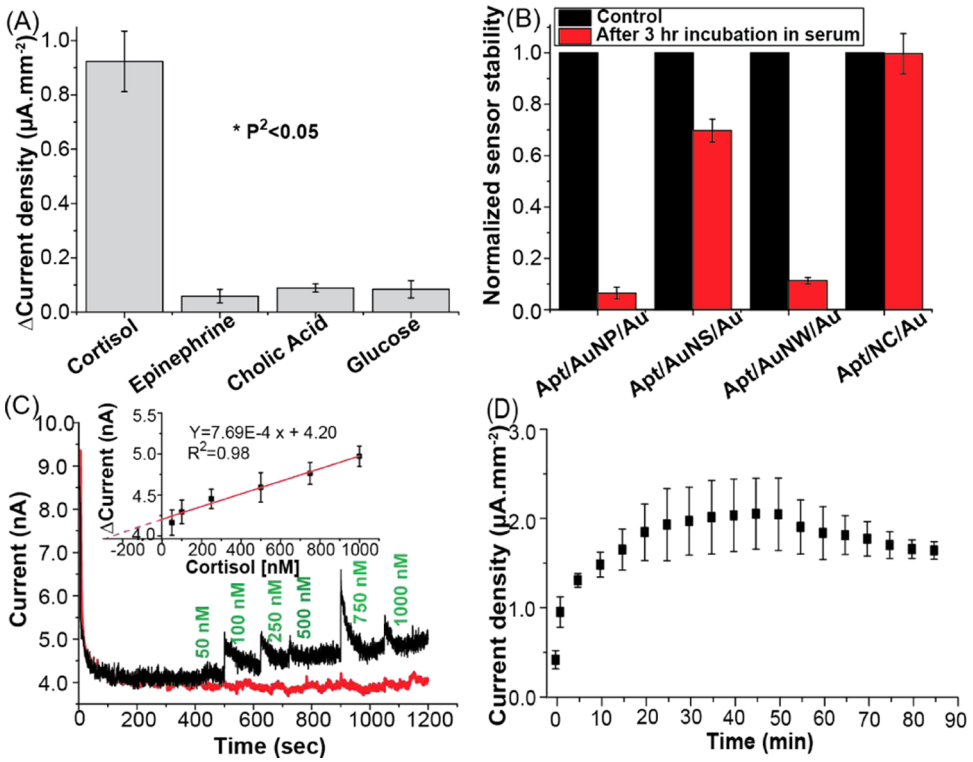


**Figure 5.** Specificity of the aptasensor and real-time response. (A) Change in current density due to off-target molecules. (B) Sensor stability in serum compared with those in other nanomaterial-based aptasensors. (C) Chronoamperometry response of the aptasensor with calibration plot (inset) as a function of cortisol concentration (black) and without cortisol (red) in 1× PBS with a 0.2 M KCl solution at −0.26 V versus Ag/AgCl. (D) Aptamer dynamic binding characteristics.

**Table 1. Performance Comparison of Existing State-of-the-Art Cortisol Aptasensors**

| method | probe | surface | test matrix | DR (nM) | LOD (nM) |
|---|---|---|---|---|---|
| colorimetric aggregation of AuNP[37] | aptamer | AuNP | serum | 150−600 | 29.5 |
| electrochemistry (amperometry) triamcinolone competitive assay[38] | aptamer | graphene-modified glassy carbon electrode | saliva and serum | 0.1−32 000 | 0.032 |
| aptamer-based lateral flow assay[40] | aptamer−AuNP | cysteamine/nitrocellulose | sweat | 32−327 | 2.7 |
| aptamer-based lateral flow assay[13] | aptamer−AuNP | nitrocellulose | diluted saliva | 0.41−41 | 1.01 |
| copper porphyrin-printed electrode[41] | aptamer−magnetic particle | multiwalled carbon nanotubes/copper/porphyrin | saliva | 1.6−65.0 | 1.0 |
| CNT−nanogap FET[39] | aptamer | multiwalled carbon nanotube | serum (10× diluted) | 0.1−2000 | 50 |
| surface plasmon resonance (SPR)[42] | aptamer | gold/titanium layer over glass | sweat | 82−16 500 | 32 |
| electrochemistry (EIS)[43] | aptamer | mercaptohexanol over gold electrode | sweat | 5−30 | 5 |
| electrochemistry (DPV) antibody−AuNP prelabeled cortisol[58] | aptamer−antibody with AuNP | MWCNTs/CMK-3/AgNP/AuNP | saliva (10× diluted) | 0.00002−276 | $3 \times 10^{-7}$ |
| electrochemistry (DPV) (this work) | structure-switching aptamer−MB | AuNW/BSA/GA over gold electrode | serum | 1−1000 | 0.68 |

The performance of the aptasensor was tested for real-time detection of cortisol in buffer with chronoamperometry. As depicted in Figure 5C, the aptasensor responded to increasing concentrations from 50 to 1000 nM in measurement buffer with well-defined chronoamperograms. The control experiment was performed in similar conditions in the absence of cortisol (red line). The kinetics followed a diffusion-limited process with a concentration-dependent increase in the current described by the Cottrell equation ($I = nFAc_0\sqrt{D/\Pi t}$), where the current, $I$, depends on the number of electrons, $n$, transferred per MB molecule on the electrode area, $A$, for a cortisol concentration $c_0$ with a diffusion coefficient, $D$. Chronoamperometry is less sensitive than DPV; hence, concentrations less than 50 nM did not show a measurable response. The aforementioned range of real-time detection (*i.e.* 50−1000 nM) is sufficient for analyzing clinical samples. The


https://doi.org/10.1021/acsomega.1c03552
ACS Omega 2021, 6, 27888−27897

calibration curve shown in the inset of Figure 5C exhibits good sensitivity (0.769 pA/[cortisol]/nM) and linearity ($R^2$ = 0.98). These data provide proof that the developed aptasensor is suitable for real-time monitoring applications.

The sensor regeneration capability was analyzed with a time-dependent DPV response through aptamer association and dissociation in buffer (Figure 5D). The binding of cortisol with the aptasensor led to increased current density, reaching a steady-state level after 50 min. After plateauing, the cortisol-spiked buffer was replaced with measurement buffer, and unbinding of the target from the aptasensor was observed, indicating partial recovery response by the aptasensor. An increase in binding affinity of the surface-immobilized aptamer[21,42] and the absence of washing or chaotropic agents in the buffer are possible reasons for the partial recovery.[31,39] Fitted globally with a 1:1 kinetic binding model, an association rate ($k_{on}$) of $1.16 \times 10^5$ $M^{-1}$ $s^{-1}$ and a dissociation rate ($k_{off}$) of $8.03 \times 10^{-1}$ $s^{-1}$ were measured.

**Performance Comparison.** A comparison of the reported aptasensor and state-of-the-art aptamer-based assays is summarized in Table 1. Huang et al. reported a sensitive technique with a very low LOD (~0.3 fM) using an aptamer−antibody hybrid assay; however, this high sensitivity required a long assay time and prelabeling of cortisol with a gold nanoparticle (AuNP)-conjugated antibody.[58] Sanghavi et al. reported an aptasensor based on the competitive displacement of electroactive species with a low LOD (~32 pM) and a wide dynamic (DR) range (100 pM to 32 $\mu$M); however, it is not suitable for long-term, continuous detection.[38] Xu et al. reported a similar dynamic range with higher LOD using a nanogap-based FET sensor with an aptamer-immobilized carbon nanotube (CNT) as a bridge but in 10-fold diluted serum.[39] Our approach's strength and novelty lie in using a conductive antifouling layer with a conformation-changing aptamer to provide good sensitivity even after prolonged exposure in undiluted serum. The conformation switching of the MB-tagged aptamer in the presence of a target allows for reagent-less, real-time detection.

## CONCLUSIONS

A novel aptasensor with enhanced antifouling properties for continuous, reagent-less, and selective detection of the stress biomarker cortisol in undiluted human serum samples is reported. The proposed sensor utilizes a 3D nanocomposite matrix offering antifouling and ease of aptamer immobilization with high sensitivity in complex biofluids. The aptasensor demonstrated a rapid response time (<30 s), a sub-nanomolar level limit of detection (0.68 nM), and a wide dynamic range (1−1000 nM) in undiluted human serum samples. Although clinical validation is needed to establish the clinical utility, the findings of studies are promising and encouraging. These attributes (*i.e.* reagent-less, wash-free continuous monitoring without surface biofouling) make it a suitable approach to integrate with implantable devices[20] to fulfill the unmet need for real-time stress monitoring. Notably, cortisol levels fluctuate throughout the day based on internal and external milieu; hence, an implantable device with continuous monitoring is needed for longitudinal, real-time assessment. We envision that the advent of improved state-of-the-art wireless implantable devices will help integrate the developed aptasensor for application in continuous wireless monitoring with the implantable biosensor.

## ASSOCIATED CONTENT

### Supporting Information

The Supporting Information is available free of charge at https://pubs.acs.org/doi/10.1021/acsomega.1c03552.

Detailed AFM and electrochemical sensor characterization, signal-to-noise ratio for cortisol detection in buffer/serum, sensor accuracy and precision studies, interfacial electron transfer characteristics and comparative nanomaterial sensor characterization studies, characterization and comparison of various nanomaterial sensors, DPV voltammogram, and buffer composition (PDF)

## AUTHOR INFORMATION


### Corresponding Author

**Drew A. Hall** − *Department of Electrical and Computer Engineering, University of California—San Diego, La Jolla, California 92093, United States; Department of Bioengineering, University of California—San Diego, La Jolla, California 92093, United States;* orcid.org/0000-0003-0674-074X; Email: drewhall@ucsd.edu

### Authors

**Naveen K. Singh** − *Department of Electrical and Computer Engineering, University of California—San Diego, La Jolla, California 92093, United States*

**Saeromi Chung** − *Department of Electrical and Computer Engineering, University of California—San Diego, La Jolla, California 92093, United States;* orcid.org/0000-0002-6389-9709

**Michael Sveiven** − *Department of Bioengineering, University of California—San Diego, La Jolla, California 92093, United States*

Complete contact information is available at: https://pubs.acs.org/10.1021/acsomega.1c03552


### Notes

The authors declare no competing financial interest.

## ABBREVIATIONS

MB-methylene blue; DPV-differential pulse voltammetry; NC-nanocomposite; EIS-electrochemical impedance spectroscopy

## REFERENCES


(1) Steckl, A. J.; Ray, P. Stress Biomarkers in Biological Fluids and Their Point-of-Use Detection. *ACS Sens.* **2018**, 2025−2044.

(2) Goh, J.; Pfeffer, J.; Zenios, S. A. The Relationship Between Workplace Stressors and Mortality and Health Costs in the United States. *Manage. Sci.* **2016**, *62*, 608−628.

(3) Wiegner, L.; Hange, D.; Björkelund, C.; Ahlborg, G. Prevalence of perceived stress and associations to symptoms of exhaustion, depression and anxiety in a working age population seeking primary care - an observational study. *BMC Fam. Pract.* **2015**, *16*, No. 38.

(4) Nater, U. M.; Skoluda, N.; Strahler, J. Biomarkers of Stress in Behavioural Medicine. *Curr. Opin. Psychiatry* **2013**, *26*, 440−445.

(5) Horowitz, M. J. Stress-response Syndromes: A Review of Posttraumatic and Adjustment Disorders. *Psychiatr. Serv.* **1986**, *37*, 241−249.

(6) Fulford, R.; Stone, G.; Fulford, D. R. *Dr. Fulford's Touch of Life: The Healing Power of the Natural Life Force*, 1st ed.; Gallery Books: New York, 1997; pp 25−50.

(7) Sakihara, S.; Kageyama, K.; Oki, Y.; Doi, M.; Iwasaki, Y.; Takayasu, S.; Moriyama, T.; Terui, K.; Nigawara, T.; Hirata, Y.; Hashimoto, K.; Suda, T. Evaluation of plasma, salivary, and urinary

cortisol levels for diagnosis of Cushing's syndrome. *Endocr. J.* **2010**, *57*, 331−337.
(8) Almadi, T.; Cathers, I.; Chow, C. M. Associations among work-related stress, cortisol, inflammation, and metabolic syndrome. *Psychophysiology* **2013**, *50*, 821−830.
(9) Straub, R. H.; Vogl, D.; Gross, V.; Lang, B.; Schölmerich, J.; Andus, T. Association of humoral markers of inflammation and dehydroepiandrosterone sulfate or cortisol serum levels in patients with chronic inflammatory bowel disease. *Am. J. Gastroenterol.* **1998**, *93*, 2197−2202.
(10) Nater, U. M.; Skoluda, N.; Strahler, J. Biomarkers of stress in behavioural medicine. *Curr. Opin. Psychiatry* **2013**, *26*, 440−445.
(11) Kaushik, A.; Vasudev, A.; Arya, S. K.; Pasha, S. K.; Bhansali, S. Recent advances in cortisol sensing technologies for point-of-care application. *Biosens. Bioelectron.* **2014**, *53*, 499−512.
(12) Upasham, S.; Prasad, S. SLOCK (sensor for circadian clock): passive sweat-based chronobiology tracker. *Lab Chip* **2020**, *20*, 1947−1960.
(13) Dalirirad, S.; Han, D.; Steckl, A. J. Aptamer-Based Lateral Flow Biosensor for Rapid Detection of Salivary Cortisol. *ACS Omega* **2020**, *5*, 32890−32898.
(14) Appel, D.; Schmid, R. D.; Dragan, C. A.; Bureik, M.; Urlacher, V. B. A fluorimetric assay for cortisol. *Anal. Bioanal. Chem.* **2005**, *383*, 182−186.
(15) Mason, S. R.; Ward, L. C.; Reilly, P. E. B. Fluorimetric detection of serum corticosterone using high-performance liquid chromatography. *J. Chromatogr. B: Biomed. Sci. Appl.* **1992**, *581*, 267−271.
(16) Lee, S.; Hwan, S. L.; Hye, J. S.; Seol, A. K.; Jimyeong, P.; Hyu, C. K.; Hyogyeong, K.; Hyung, J. K.; Yun, T. K.; Kyoung, R. L.; Young, J. K. Simultaneous Determination of Cortisol and Cortisone from Human Serum by Liquid Chromatography-Tandem Mass Spectrometry. *J. Anal. Methods Chem.* **2014**, No. 787483.
(17) Stevens, R. C.; Soelberg, S. D.; Near, S.; Furlong, C. E. Detection of Cortisol in Saliva with a Flow-Filtered, Portable Surface Plasmon Resonance Biosensor System. *Anal. Chem.* **2008**, *80*, 6747−6751.
(18) Zhou, J. C.; Maria, H. C.; Esther, H. L.; Bruce, D.; Patricia, L. G.; Scott, M. S. Immunoassays for cortisol using antibody-doped sol−gel silica. *J. Mater. Chem.* **2004**, *14*, 2311−2316.
(19) Barfidokht, A.; Mishra, R. K.; Seenivasan, R.; Shuyang, L.; Lee, J. H.; Wang, J.; Hall, D. A. Wearable electrochemical glove-based sensor for rapid and on-site detection of fentanyl. *Sens. Actuators, B* **2019**, *296*, No. 126422.
(20) Jiang, H.; Zhou, X.; Kulkarni, S.; Uranian, M.; Seenivasan, R.; Hall, D. A. In *A Sub-1 μW Multiparameter Injectable BioMote for Continuous Alcohol Monitoring*, 2018 IEEE Custom Integrated Circuits Conference (CICC), 2018; pp 1−4.
(21) Singh, N. K.; Arya, S. K.; Estrela, P.; Goswami, P. Capacitive malaria aptasensor using Plasmodium falciparum glutamate dehydrogenase as target antigen in undiluted human serum. *Biosens. Bioelectron.* **2018**, *117*, 246−252.
(22) Sun, A. C.; Hall, D. A. Point-of-Care Smartphone-based Electrochemical Biosensing. *Electroanalysis* **2019**, *31*, 2−16.
(23) Venkatesh, A. G.; Brickner, H.; Looney, D.; Hall, D. A.; Aronoff, S. E. Clinical detection of Hepatitis C viral infection by yeast-secreted HCV-core:Gold-binding-peptide. *Biosens. Bioelectron.* **2018**, *119*, 230−236.
(24) Wang, J. Electrochemical biosensors: Towards point-of-care cancer diagnostics. *Biosens. Bioelectron.* **2006**, *21*, 1887−1892.
(25) Mokhtari, Z.; Habibollah, K.; Sedigheh, H.; Solati, R.; Shahrokhian, S.; et al. Evaluation of molecular imprinted polymerized methylene blue/aptamer as a novel hybrid receptor for Cardiac Troponin I (cTnI) detection at glassy carbon electrodes modified with new biosynthesized ZnONPs. *Sens. Actuators, B* **2020**, *320*, No. 128316.
(26) Plaxco, K. W.; Soh, H. T. Switch-based biosensors: a new approach towards real-time, in vivo molecular detection. *Trends Biotechnol.* **2011**, *29*, 1−5.
(27) Veerapandian, M.; Hunter, R.; Neethirajan, S. Dual immunosensor based on methylene blue-electroadsorbed graphene oxide for rapid detection of influenza virus antigen. *Talanta* **2016**, *155*, 250−257.
(28) Jain, P.; Chakma, B.; Singh, N. K.; Patra, S.; Goswami, P. Aromatic Surfactant as Aggregating Agent for Aptamer-Gold Nanoparticle-Based Detection of Plasmodium Lactate Dehydrogenase. *Mol. Biotechnol.* **2016**, *58*, 497−508.
(29) Singh, N. K.; Chakma, B.; Jain, P.; Goswami, P. Protein-Induced Fluorescence Enhancement Based Detection of Plasmodium falciparum Glutamate Dehydrogenase Using Carbon Dot Coupled Specific Aptamer. *ACS Comb. Sci.* **2018**, *20*, 350−357.
(30) Singh, N. K.; Ray, P.; Carlin, A. F.; Magallanes, C.; Morgan, S. C.; Laurent, L. C.; Aronoff, E. S.; Hall, D. A. Hitting the diagnostic sweet spot: Point-of-care SARS-CoV-2 salivary antigen testing with an off-the-shelf glucometer. *Biosens. Bioelectron.* **2021**, *180*, No. 113111.
(31) Radi, A. E.; Acero, J. L.; Baldrich, E.; Sullivan, C. K. Reagentless, Reusable, Ultrasensitive Electrochemical Molecular Beacon Aptasensor. *J. Am. Chem. Soc.* **2006**, *128*, 117−124.
(32) Chung, S.; Sicklick, J. K.; Ray, P.; Hall, D. A. Development of a Soluble KIT Electrochemical Aptasensor for Cancer Theranostics. *ACS Sens.* **2021**, *6*, 1971−1979.
(33) Villalonga, A.; Pérez-Calabuig, A. M.; Villalonga, R. Electrochemical biosensors based on nucleic acid aptamers. *Anal. Bioanal. Chem.* **2020**, *412*, 55−72.
(34) Russo, M. J.; Mingyu, H.; Pauline, E. D.; Clayton, S. M.; Jessair, D.; Anita, F. Q.; Robert, M. K.; Simon, E. M.; Rosanne, M. G.; George, W. G.; Saimon, M. S. Antifouling Strategies for Electrochemical Biosensing: Mechanisms and Performance toward Point of Care Based Diagnostic Applications. *ACS Sens.* **2021**, *6*, 1482−1507.
(35) Barfidokht, A.; Gooding, J. J. Approaches Toward Allowing Electroanalytical Devices to be Used in Biological Fluids. *Electroanalysis* **2014**, *26*, 1182−1196.
(36) Gooding, J. J. Finally, a simple solution to biofouling. *Nat. Nanotechnol.* **2019**, *14*, 1089−1090.
(37) Martin, J. A.; Chávez, J. L.; Chushak, Y.; Chapleau, R. R.; Hagen, J.; Kelley, L. N. Tunable stringency aptamer selection and gold nanoparticle assay for detection of cortisol. *Anal. Bioanal. Chem.* **2014**, *406*, 4637−4647.
(38) Sanghavi, B. J.; John, A. M.; Jorge, L. C.; Joshua, A. H.; Kelley, N. L.; Chia, F. C.; Nathan, S. Aptamer-functionalized nanoparticles for surface immobilization-free electrochemical detection of cortisol in a microfluidic device. *Biosens. Bioelectron.* **2016**, *78*, 244−252.
(39) Xu, X.; Pierrick, C.; Johnas, E. O.; Kelley, N. L.; Kasper, M. P.; Jorge, L. C.; Matteo, P. Reconfigurable Carbon Nanotube Multiplexed Sensing Devices. *Nano Lett.* **2018**, *18*, 4130−4135.
(40) Dalirirad, S.; Steckl, A. J. Aptamer-based lateral flow assay for point of care cortisol detection in sweat. *Sens. Actuators, B* **2019**, *283*, 79−86.
(41) Fernandez, R. E.; Umasankar, Y.; Manickam, P.; Nickel, J.; Iwasaki, L.; Kawamoto, B. K.; Todoki, K. C.; Scott, J. M.; Bhansali, S. Disposable aptamer-sensor aided by magnetic nanoparticle enrichment for detection of salivary cortisol variations in obstructive sleep apnea patients. *Sci. Rep.* **2017**, *7*, No. 17992.
(42) Hwang, Y.; Gupta, N. K.; Ojha, Y. R.; Cameron, B. D. In *An Optical Sensing Approach for the Noninvasive Transdermal Monitoring of Cortisol*, Proceedings of SPIE, Nanoscale Imaging, Sensing, and Actuation for Biomedical Applications, 2016; Vol. *8*, p 97210.
(43) Pilehvar, S.; Lin, S.; Hojaiji, H.; Zhao, Y.; Emaminejad, S. Highly senstive impediometric aptasensor for werable detection of hormones. *Solid-State Sens.* **2018**, *978*, No. 940470-03.
(44) Yang, K. A.; Hyosun, C.; Yameng, Z.; Stevan, P.; Nako, N.; Anne, M. A.; Tilla, S. W.; Milan, N. S. High-Affinity Nucleic-Acid-Based Receptors for Steroids. *ACS Chem. Biol.* **2017**, *12*, 3103−3112.
(45) Sabaté del Río, J.; Henry, O. Y. F.; Jolly, P.; Ingber, D. E. An antifouling coating that enables affinity-based electrochemical biosensing in complex biological fluids. *Nat. Nanotechnol.* **2019**, *14*, 1143−1149.


https://doi.org/10.1021/acsomega.1c03552
*ACS Omega* 2021, 6, 27888−27897

(46) Chatterjee, S.; Sengupta, K.; Bandyopadhyay, S.; Dey, A. Ammonium tetrathiomolybdate as a novel electrode material for convenient tuning of the kinetics of electrochemical $O_2$ reduction by using iron−porphyrin catalysts. *J. Mater. Chem. A* **2016**, *4*, 6819−6823.
(47) Fotouhi, L.; Hashkavayi, A. B.; Heravi, M. M. Electrochemical behaviour and voltammetric determination of sulphadiazine using a multi-walled carbon nanotube composite film-glassy carbon electrode. *J. Exp. Nanosci.* **2013**, *8*, 947−956.
(48) Shrivastava, A.; Gupta, V. Methods for the determination of limit of detection and limit of quantitation of the analytical methods. *Chron. Young Sci.* **2011**, *2*, 21.
(49) Bang, G. S.; Cho, S.; Kim, B. G. A novel electrochemical detection method for aptamer biosensors. *Biosens. Bioelectron.* **2005**, *21*, 863−870.
(50) Schoukroun-Barnes, L. R.; Florika, C. M.; Brenda, G.; Justine, L.; Juan, L.; Ryan, J. W. Reagentless, Structure-Switching, Electrochemical Aptamer-Based Sensors. *Annu. Rev. Anal. Chem.* **2016**, *9*, 163−181.
(51) Singh, N. K.; Jain, P.; Das, S.; Goswami, P. Dye Coupled Aptamer-Captured Enzyme Catalyzed Reaction for Detection of Pan Malaria and P. falciparum Species in Laboratory Settings and Instrument-Free Paper-Based Platform. *Anal. Chem.* **2019**, *91*, 4213−4221.
(52) Wang, J.; Wang, F.; Dong, S. Methylene blue as an indicator for sensitive electrochemical detection of adenosine based on aptamer switch. *J. Electroanal. Chem.* **2009**, *626*, 1−5.
(53) Kinnamon, D.; Ghanta, R.; Lin, K. C.; Muthukumar, S.; Prasad, S. Portable biosensor for monitoring cortisol in low-volume perspired human sweat. *Sci. Rep.* **2017**, *7*, No. 13312.
(54) Koutsoumpeli, E.; Murray, J.; Langford, D.; Bon, R. S.; Johnson, S. Probing molecular interactions with methylene blue derivatized self-assembled monolayers. *Sens. Bio-Sens. Res.* **2015**, *6*, 1−6.
(55) Van Loco, J.; Elskens, M.; Croux, C.; Beernaert, H. Linearity of calibration curves: use and misuse of the correlation coefficient. *Accredit. Qual. Assur.* **2002**, *7*, 281−285.
(56) Park, J. W.; Kallempudi, S. S.; Niazi, J. H.; Gurbuz, Y.; Youn, B. S.; Gu, M. B. Rapid and sensitive detection of Nampt (PBEF/visfatin) in human serum using an ssDNA aptamer-based capacitive biosensor. *Biosens. Bioelectron.* **2012**, *38*, 233−238.
(57) Hasegawa, K.; Minakata, K.; Suzuki, M.; Suzuki, O. The standard addition method and its validation in forensic toxicology. *Forensic Toxicol.* **2021**, *39*, 311−333.
(58) Huang, Z.; Hao, C.; Huarong, Y.; Zixuan; Chen, N. R.; Guo, Z. An ultrasensitive aptamer-antibody sandwich cortisol sensor for the noninvasive monitoring of stress state. *Biosens. Bioelectron.* **2021**, *190*, No. 113451.


https://doi.org/10.1021/acsomega.1c03552
*ACS Omega* 2021, 6, 27888−27897